Modeling the structural, dynamical, and magnetic properties of liquid $Al_{1-x}Mn_x$ ($x=0.14$, 0.2, and 0.4): A first-principles investigation

N. Jakse[1] and A. Pasturel[1,2]
[1]*Laboratoire Sciences et Ingénierie, Matériaux et Procédés, ENSEEG-INPG, Boîte Postale 75, 38402 Saint Martin d'Hères Cedex, France*
[2]*Laboratoire de Physique et Modélisation des Milieux Condensés, Maison des Magistères, Boîte Postale 166 CNRS, 38042 Grenoble-Cedex 09, France*

(Received 6 March 2006; revised manuscript received 26 February 2007; published 24 July 2007)

We report the results of first-principles molecular dynamics simulations of liquid $Al_{1-x}Mn_x$ alloys at three different compositions. The local structure as defined by the Bhatia-Thornton partial structure factors is found to display significant changes at $x=0.4$. In addition, a structural analysis using three-dimensional pair-analysis techniques evidences a fivefold symmetry around $x=0.14$, in agreement with the experimental quasicrystal-forming range, and an increasing complexity of the Frank-Kasper polytetrahedral symmetry around Mn atoms at $x=0.4$. We also examine the time evolution of the configurations at the three compositions in terms of the mean-square displacements and self-diffusion coefficients. Finally, we show a strong interplay between the structural changes and the evolution of the magnetic properties of the Mn atoms as a function of composition.

DOI: 10.1103/PhysRevB.76.024207 PACS number(s): 61.20.−p, 61.20.Ja, 61.25.Mv

I. INTRODUCTION

The interplay between the short-range structure of metallic liquid alloys and their electronic and magnetic properties is of both fundamental and practical interest, but it is generally much less understood than that observed in the well-defined crystalline structures. For instance, liquid $Al_{1-x}Mn_x$ alloys in the region near 20 at. % Mn are very attractive since they are known to form quasicrystalline phases under fast quenching techniques. Another remarkable observed property of these alloys is the increase of the magnetic susceptibility on melting as well as a subsequent rise with temperature in the liquid state. This behavior is quite opposite to what is expected from the usual spin-fluctuation theories where the magnetic susceptibility is Curie-like, and therefore decreases with increasing temperature.

Experimentally, Maret *et al.* performed a detailed analysis of the composition dependence of topological and chemical orders in liquid $Al_{1-x}Mn_x$ alloys ($x=0.14$, 0.2, 0.267, and 0.4) by neutron diffractions.[1] Three of these compositions ($x=0.14$, 0.2, and 0.267) are in the quasicrystal-forming range while one ($x=0.4$) is outside it. The main conclusion is that all these alloys exhibit a tendency toward icosahedral ordering even for $x=0.4$. However, the experimental evidence of the fivefold symmetry is quite indirect since it is based essentially on the overall similarity observed between the structure factors of liquid phases and their present icosahedral or equilibrium solid phases.

In addition, using low momentum transfer as well as polarized neutron-scattering experiments combined with susceptibility measurements, Hippert and co-workers[2] have established that magnetic moments appear upon melting on Mn atoms which are nonmagnetic in the solid, paramagnetism continuing to increase with increasing temperature in the liquid state. The origin of this behavior was discussed on the basis of nonhomogeneous magnetism and an evolution of the icosahedral short-range order (ISRO) when the temperature increases. Nonhomogeneous magnetism is characterized by two types of Mn atoms, magnetic and nonmagnetic; the fraction of nonmagnetic atoms display a local environment close to that in the solid, namely, an icosahedral environment, while magnetic Mn atoms have another environment. Within this assumption, the fraction of nonmagnetic Mn atoms has to decrease with increasing temperature, with the idea that the icosahedral symmetry is progressively destroyed as temperature increases.

On the theoretical side, there have been several attempts to study the local structure and the magnetic properties of liquid Al-Mn alloys using molecular-dynamics simulations coupled with either pair potentials proposed by Philips *et al.*[3,4] or interatomic tight-binding-based potentials.[5–7] However the exact nature of the magnetic states of Mn atoms was under debate mainly due to the semiempirical forms of the interatomic interactions. It is clear that a powerful simulation of the electronic and magnetic properties of Al-T (where T is a transition metal) alloys requires an accurate description of Al-T bonds which are beyond the scope of these semiempirical approaches. To circumvent this difficulty, interatomic potentials derived from neutron-diffraction data in the liquid state have been coupled with molecular-dynamics simulations to characterize the local symmetry of liquid $Al_{80}Mn_{20}$ and $Al_{60}Mn_{40}$ alloys.[8] Using an analysis based on Voronoi polyhedra, the authors concluded that topological ordering in both liquids is mainly formed by the same type of local symmetry. However, it is quite obvious that the fitted pair potentials are unable to capture the variations of the complex electronic effects as a function of composition and/or temperature.

As an alternative, one can use first-principles electronic structure calculations to capture the exact nature of SRO in such liquid alloys and to have an accurate description of their electronic and magnetic properties. Very recently,[9] we investigated the structural properties of $Al_{80}Mn_{20}$ and $Al_{80}Ni_{20}$ alloys above and below their experimental liquidus temperatures using first-principles molecular-dynamics (MD) simulations coupled to a structural analysis based on three-

dimensional pair-analysis techniques.[10] We have also studied the formation of magnetic moments in liquid $Al_{80}Mn_{20}$ alloys as a function of temperature.[11] Our findings showed that the local structure of $Al_{80}Mn_{20}$ and $Al_{80}Ni_{20}$ alloys is characterized by a strong Al-T affinity, leading to a well-pronounced chemical short-range order (CSRO) in both alloys. However, from the structural analysis using bonding orientational order and three-dimensional pair-analysis technique, our results clearly pointed out the predominance of fivefold symmetry around Mn atoms, while the local environment of Ni atoms is characterized by a close-packed local symmetry more pronounced than the fivefold symmetry. Concerning magnetic properties of $Al_{80}Mn_{20}$ alloys as a function of temperature, we have obtained the result that calculated magnetic moments on Mn atoms are not sensitive to interactions with other Mn as found experimentally.[2] However, our results do not confirm the experimental view that only a fraction of Mn sites carry a moment due to a strong local environment effect, with others being nonmagnetic. On the contrary, we obtained the result that calculated Mn moments are close to those obtained from the single-impurity mode, the small distribution being related to thermal fluctuations which favor atomic displacements. Finally, we showed that thermal expansion effects mainly explain the continuous increase of magnetism with temperature.

Given that the structural and magnetic properties of Al-Mn systems in the liquid state can be successfully described using first-principles MD simulations,[9,11] in this paper we address the question of the evolution of the local structure as well as the magnetic state of Mn atoms as a function composition by performing a series of simulations for $x=0.14$, 0.2, and 0.4. Our *ab initio* MD results show significant changes of the local structure at $x=0.4$ characterized by a strong shortening of the Mn-Mn distances in perfect agreement with experimental trends. By refining our study of the structural properties with the common-neighbor three-dimensional analysis,[10] our findings further indicate the predominance of the icosahedral symmetry around $x=0.14$ in agreement with the experimental quasicrystal-forming range. A dynamical image is proposed by analyzing the particularities of the mean-square displacement as well as the self-diffusion coefficients of each species for the three compositions. Finally, we show that the composition dependence of magnetism in the $Al_{1-x}Mn_x$ alloys can be related to the evolution of the local environment of the Mn atoms.

The outline of the paper is the following. In Sec. II, we describe the computational methods. Section III is devoted to the results and their discussion. A brief summary and conclusions are given in Sec. IV.

II. COMPUTATIONAL DETAILS

A. First-principles calculations

Our first-principles calculations are based on density functional theory using the form of generalized gradient approximation developed by Perdew and Wang.[12] We use the most recent version of the Vienna *ab initio* simulation package[13] (VASP) in which the interactions between the ions and electrons are described by the projector augmented-wave (PAW) method.[14] In the present PAW potentials, the 4*s* and 3*d* orbitals are treated as valence orbitals for Mn while 3*s* and 3*p* orbitals are used as valence orbitals for Al, with a plane-wave cutoff of 270 eV. In the simulations, we have treated the spin variable explicitly with the gradient-corrected local spin density approximation[15] since, in our previous work,[9] we have shown that an explicit spin treatment is necessary to obtain a correct description of the experimental partial pair-correlation function $G_{\mathrm{MnMn}}(r)$.

TABLE I. Temperatures T and number densities ρ used in the simulations, which correspond to the experimental data of Ref. 1. The values of D and N are, respectively, the self-diffusion coefficients and the coordination numbers in $Al_{1-x}Mn_x$ liquids.

	x		
	0.14	0.20	0.40
T (K)	1330	1380	1510
ρ (Å^{-3})	0.054	0.058	0.064
D_{Mn} (Å^2 ps^{-1})	0.31	0.27	0.23
D_{Al} (Å^2 ps^{-1})	0.67	0.46	0.29
N_{tot}	12.49	13.15	13.46
N_{Mn}	11.90	12.56	13.21
N_{Al}	12.59	13.28	13.63
$N_{\mathrm{Mn\text{-}Mn}}$	1.10	1.97	4.53
$N_{\mathrm{Al\text{-}Al}}$	10.82	10.65	7.87
$N_{\mathrm{Mn\text{-}Al}}$	10.80	10.58	8.69

B. Molecular dynamics and inherent structures

We have considered a system of 256 atoms in a cubic box with periodic boundary conditions. To study the composition dependence of the local structure of liquid $Al_{1-x}Mn_x$ alloys, we have performed three MD simulations for composition $x=0.14$ (36 Mn, 220 Al), 0.2 (51 Mn, 205 Al), and 0.4 (102 Mn, 154 Al) at temperatures $T=1330$, 1380, and 1510 K, respectively. For each composition, the volume of the cell has been fixed to reproduce the experimental densities given in Ref. 1 just above the liquidus (see the values in Table I). It is worth mentioning that it results in lengths of the simulation box $L=16.799$, 16.403, and 15.874 Å, respectively, for $x=0.14$, 0.2, and 0.4, and that these finite-size effects have been examined in a previous contribution.[16] Only the Γ point was considered to sample the supercell Brillouin zone. Tests to study the influence of Brillouin-zone sampling are very difficult to perform since *ab initio* simulations using many k points are very demanding. However, Alfe *et al.*[17] have shown indirectly that the Γ point is sufficient for the cell size used. Moreover, we must emphasize that the present study focuses on the evolution of some properties as a function of composition, and errors due to the size of the simulated system and the k-point sampling were found to be negligible compared to the composition effects. All the dynamical simulations were carried out in the canonical ensemble (*NVT*) by means of a Nosé thermostat with a characteristic frequency equal to 38 ps^{-1}. Newton's equations of motion

were integrated using the Verlet algorithm in the velocity form with a time step of 3 fs. The procedure of the simulations is the following: the initial positions are obtained from tight-binding molecular-dynamics simulations;[5] after an equilibration period of 6 ps, with a total simulation time of 27 ps. A 2000 configurations were used to produce averaged structural quantities such as the partial pair-correlation functions. Among these configurations, ten selected ones, regularly spaced in time, are saved to extract their inherent structures.[18] To this end, the steepest-descent energy-minimization procedure with the conjugate gradient method is imposed on each of these configurations. This method allows us to uncouple the vibrational motion from the underlying structural properties since atoms are brought to a local minimum in the potential-energy surface. At $x=0.2$ and $T=1380$ K, the simulation done in the present work is an extension of the one made in the previous study.[9]

III. RESULTS AND DISCUSSION

In order to analyze the simulations described above, we have calculated several structural and magnetic quantities in order to emphasize their evolution as a function of composition.

First, to assess the quality of the simulations, the mean-square displacement (MSD) $\langle R^2(t)\rangle$ is calculated at time t as

$$\langle R_i^2(t)\rangle = \langle[\vec{r}_i(t) - \vec{r}_i(0)]^2\rangle \quad (1)$$

about an arbitrary time origin, for each species i. In Fig. 1, the MSD is drawn for the three compositions and for each species. It reveals three distinctive regimes in the individual motion of the atoms: a ballistic motion seen at very short times, in which the atoms evolve as t^2, followed by a cross-over region, where the slope of $\langle R^2(t)\rangle$ weakens. The latter is interpreted as a slowing down of the motion of the atoms as they encounter their first neighbors, and is called the cage effect. Finally, at long times, typically after 1 ps for the three systems studied here, the atoms enter a diffusive regime in which the mean-square displacement grows linearly with time. The diffusive regime is sufficiently long for an accurate statistical analysis in the liquid state

The self-diffusion coefficients for each species have been estimated from the velocity autocorrelation functions (not shown) and gathered in Table I. To our best knowledge the self-diffusion coefficients have been neither measured nor calculated by MD simulations. Nevertheless, self-diffusion coefficients have been determined using *ab initio* MD simulation for a similar system,[19] namely, $Al_{80}Ni_{20}$ at $T=1300$ K. It appears that the values for Ni and Al are close to those found here for Mn and Al, respectively.[16] As the concentration of Mn atoms increases, the values of D_{Mn} and D_{Al} decrease, with the difference between the two coefficients becoming small for $x=0.40$. This can be interpreted by the fact that, as the heavier Mn atoms become more numerous, the Al atoms experience a more marked cage effect, as can be seen in Fig. 1(c) and induce a slowing down of their motion. This phenomenon is amplified by the increase of the density.

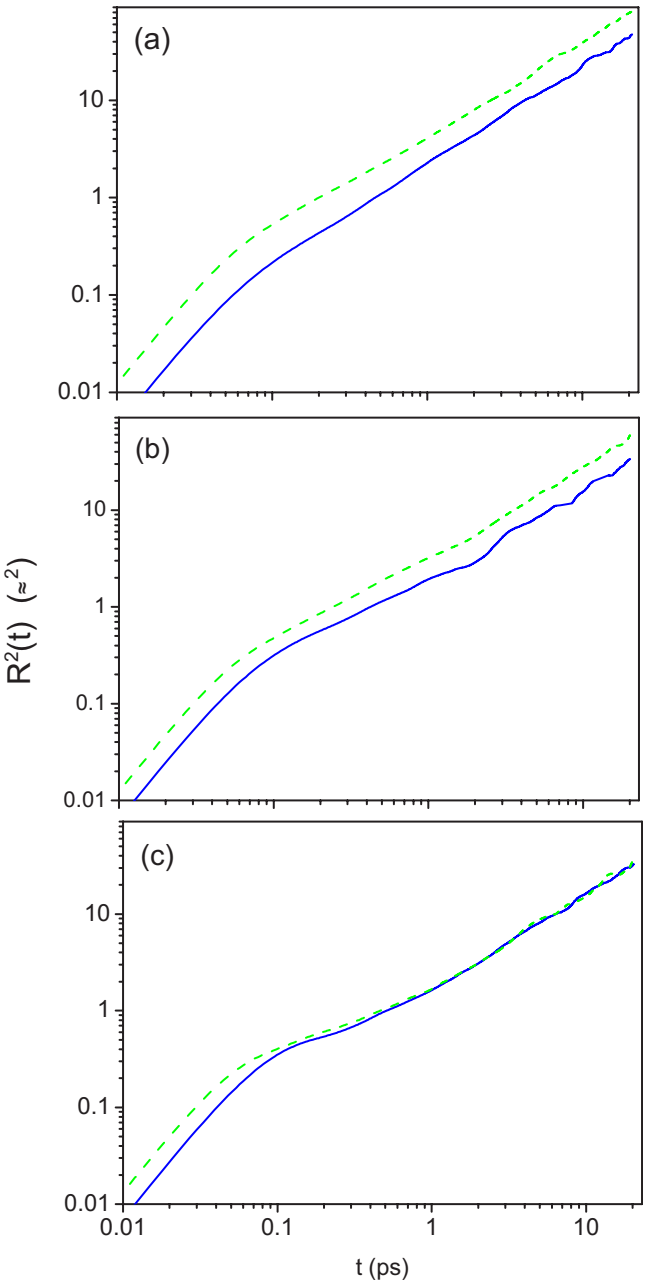

FIG. 1. (Color online) Mean-square displacement for $Al_{1-x}Mn_x$ liquids at concentration $x=0.14$ (a), 0.2, (b), and 0.4 (c): the solid and dashed lines correspond to the Mn and Al atoms, respectively.

We come now to the calculation of the structural quantities in order to emphasize their evolution as a function of composition. For the three alloys $Al_{1-x}Mn_x$ with $x=0.14$, 0.20, and 0.40, we have considered the Bhatia-Thornton partial structure factors in Figs. 2 and 3 and the functions $G_{ij}(r)$ in Fig. 4, the latter being related to the partial pair-correlation functions $g_{ij}(r)$ by $G_{ij}(r)=r[g_{ij}(r)-1]$, i and j representing the species of atoms. The functions $g_{ij}(r)$ have been calculated beyond $r=L/2$ using the method of Baranyai and Evans.[20] We have determined the nearest-neighbor coordination numbers z^1_{AlAl}, z^1_{AlMn}, and z^1_{MnMn} by counting the numbers of atoms in the first coordination shells directly from the configurations, which is equivalent to integrating the radial

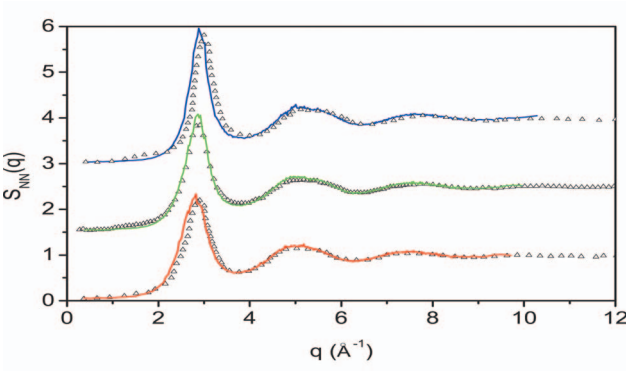

FIG. 2. (Color online) Number-number structure factors $S_{NN}(q)$ for $Al_{1-x}Mn_x$ liquids: the solid lines correspond to the MD simulations and the triangles are experimental data from Ref. 1. The curves for $x=0.2$ and 0.4 are shifted upward by amounts of 1.5 and 3, respectively.

distribution functions $\mathcal{R}_{ij}(r)=c_j 4\pi\rho r^2 g_{ij}(r)$ (ρ being the atomic density) up to the first minimum of $g_{ij}(r)$. For the latter as well as for the common-neighbor analysis below, a mean value of 3.9 Å for $x=0.14$ and 0.2 and 3.8 Å for $x=0.4$ has been taken. The partial nearest-neighbor distances r_{AlAl}, r_{AlMn}, and r_{MnMn} have been estimated[9] from the first maxima of the $g_{ij}(r)$'s. All these values are compiled in Table II.

The Bhatia-Thornton partial structure factors are especially useful for displaying the short-range order in a binary liquid alloy. These are obtained from the partial structure factors

$$S_{ij}(q) = \frac{1}{\sqrt{N_i N_j}} \left\langle \sum_{k}^{N_i} \sum_{l}^{N_j} \exp[-i\vec{q}\cdot(\vec{r}_{i,k} - \vec{r}_{j,l})] \right\rangle, \qquad (2)$$

where N_i and N_j are the numbers of atoms of species i and j. $\vec{q}=(2\pi/L)(n_x,n_y,n_z)$ are wave vectors compatible with the

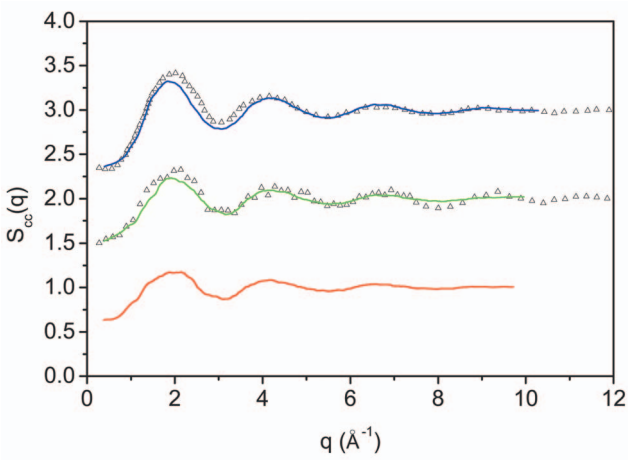

FIG. 3. (Color online) Concentration-concentration structure factors $S_{cc}(q)$ for $Al_{1-x}Mn_x$ liquids: the solid lines correspond to the MD simulations and the triangles are experimental data from Ref. 1. The curves for $x=0.2$ and 0.4 are shifted upward by amounts of 1 and 2, respectively. A smoothing has been applied to the curves using a standard adjacent-averaging technique.

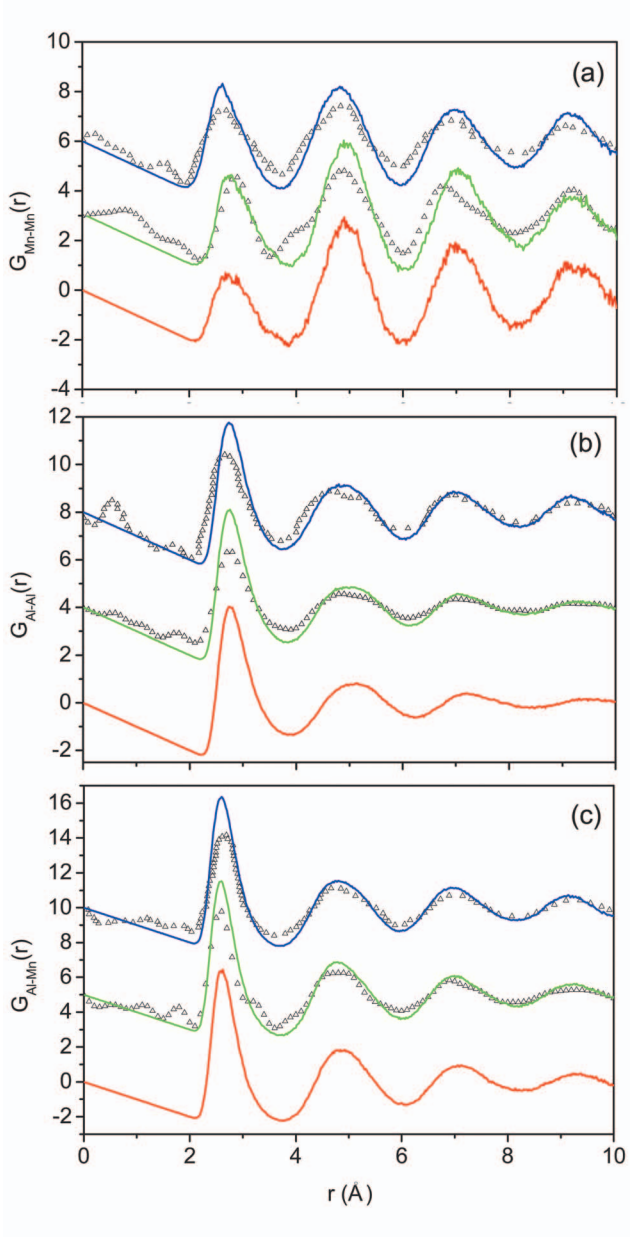

FIG. 4. (Color online) Mn–Mn (a), Al-Al (b), and Al-Mn (c) partial pair-correlation function for $Al_{1-x}Mn_x$ liquids at $x=0.14$, 0.2, and 0.4: the solid lines correspond to the MD simulations and the triangles are experimental data from Ref. 1. The curve for $x=0.2$ is shifted upwards by an amount of 3 in (a), 4 in (b), and 5 in (c) while that for $x=0.4$ is shifted upwards by an amount of 6 in (a), 8 in (b), and 10 in (c).

length L of the simulation cell, and n_x, n_y, and n_z are integers. The density-density factor $S_{NN}(q)$ describes the topological properties of the spatial arrangement of the mean atoms, i.e., the topological short-range order (TSRO) of the system, while the concentration-concentration factor $S_{cc}(q)$ describes the local fluctuations in the concentration and hence its chemical short-range order. The cross term $S_{Nc}(q)$, which couples the density and concentration variables, is related to the size difference between both alloying species.

TABLE II. Interatomic distances in $Al_{1-x}Mn_x$ liquids.

	x		
R_{ij} (Å)	0.14	0.20	0.40
Mn-Mn	2.95	2.91	2.75
Al-Al	2.75	2.76	2.74
Mn-Al	2.62	2.60	2.60

As a first step, we discuss the evolution of TSRO as a function of composition through the calculated $S_{NN}(q)$ shown in Fig. 2. For comparison, we have reported the experimental results at similar compositions.[1] A number of features deserve mention. (i) First, the position and the height of the principal peak are virtually unchanged for both $x=0.14$ and 0.2. However, the position of that peak, q_1, is considerably modified for $x=0.4$ with a shift to higher q values. The strong increase of that peak is another striking feature. This behavior is in perfect agreement with experimental features[1] and also with previous empirical simulations.[8] (ii) No significant change in the shape of the second peak of $S_{NN}(q)$ is observed. For the three alloys, we note that the second peak exhibits a shoulder on the right-hand side, leading to a rather asymmetrical shape extending from $1.7q_1$ to $2q_1$. Despite the absence of a clear second-peak splitting which is suggestive of local icosahedral order,[21] we can note that the height ratio between the first peak and the second peak for $x=0.14$ and 0.2 is equal to 0.49, similar to the theoretical value obtained by using a Landau description of short-range icosahedral order.[21] At $x=0.4$, this ratio is equal to 0.40, suggesting that the icosahedral order is less pronounced for that composition. Finally, it is worth noting that the very small amplitudes of oscillations of $S_{Nc}(q)$ (not shown) indicate that the atomic sizes of Al and Mn are close in liquid $Al_{1-x}Mn_x$.

For the three compositions, the calculated functions $S_{cc}(q)$ reproduce the experimental pronounced peak centered around 1.9 $Å^{-1}$ and which is indicative of a well-defined chemical SRO in liquid $Al_{1-x}Mn_x$ alloys (see Fig. 2). This results from a strong chemical order between Mn and Al atoms and we note that the peak is slightly more pronounced for $x=0.4$. The spatial extent of chemical ordering deduced from the breadth of the first peak is about twice as small as that of topological ordering. To obtain a more quantitative estimate for the CSRO and its dependence with composition, we consider the Warren CSRO parameter a_1 generalized by Wagner and Ruppersberg to systems with size effects.[22] α_1 is calculated using the values of z_{ij}^1 tabulated in Table I as follows:

$$\alpha_1 = 1 - z_{T\text{-Al}}^1 / c_{\text{Al}}(c_T z_{\text{Al}}^1 + c_{\text{Al}} z_{TM}^1), \tag{3}$$

with $z_i^1 = z_{ii}^1 + z_{ij}^1$ $(i,j=T,\text{Al})$, and c_j the concentration of species j. α_1 is equal to -0.047, -0.041, and -0.083 for $x=0.14$, 0.2, and 0.4, respectively. We observe a slight increase of the α_1 parameter for $x=0.4$.

Therefore, the analysis of both $S_{NN}(q)$ and $S_{cc}(q)$ shows a change of SRO at $x=0.4$. To study this composition dependence more carefully, we inspect the interatomic distances.

TABLE III. Analysis of the MD simulations in bonded pairs for $Al_{1-x}Mn_x$ liquids around Mn atoms. The abundances are averaged over the ten selected inherent configurations and the absolute error bar of the abundances is 0.01.

	x		
Mn pairs	0.14	0.20	0.40
1551	0.51	0.37	0.34
1541	0.06	0.13	0.14
1431	0.15	0.21	0.14
1421	0.01	0.02	0.01
1422	0.01	0.05	0.02
1201	0.00	0.00	0.00
1211	0.00	0.00	0.00
1301	0.00	0.00	0.00
1311	0.01	0.02	0.01
1321	0.01	0.02	0.02
1331	0.01	0.00	0.02
1441	0.13	0.08	0.08
1661	0.07	0.06	0.12
2101	1.79	1.71	1.99
2211	1.16	1.08	1.15
2321	0.03	0.06	0.09
2331	0.85	0.76	1.08
2441	0.08	0.11	0.25

As observed in Table II, the most salient feature is the shortening of the first Mn-Mn interatomic distances in $Al_{60}Mn_{40}$ while Al-Al and Al-Mn distances display negligible variation as a function of composition. Thus the first distance Mn-Mn in $Al_{60}Mn_{40}$ becomes comparable to other Mn-Al and Al-Al distances, which perfectly follows the experimental trend.[1] This is illustrated also in Fig. 3, where $G_{\text{Al-Mn}}(r)$, $G_{\text{Mn-Mn}}(r)$, and $G_{\text{Al-Al}}(r)$ are in overall good agreement with the experiment for both compositions.

To obtain more detailed information about the origin of the evolution of the local atomic structure at $x=0.4$, we use the common-neighbor (CN) analysis applied to pairs involving at least one Mn atom, since we have shown that the Mn-Mn distances have a different behavior in $Al_{80}Mn_{20}$ and $Al_{80}Mn_{40}$ alloys. For each composition, Table III contains the relative abundance of selected pairs, averaged over the ten inherent configurations. A set of four indices is associated with each of them:[10] (i) the first index denotes to what peak of $g(r)$ the pair under consideration belongs, i.e., the root pair, (ii) the second index represents the number of near neighbors shared by the root pair, (iii) the third index is for the number of nearest-neighbor bonds among the shared neighbors; and (iv) the fourth index is used to distinguish configurations with the same first three indices but with a different topology. This method is able to distinguish between various local structures like fcc, hcp, bcc, and icosahedral environments. For example, four bonded pairs are represented in a bulk fcc crystal as 1421, 2101, 2211, and 2441. A bulk hcp crystal contains the same pairs but not with

the same weight, and additional pairs like 1422 and 2331 pairs. 1441, 1661, 2101, 2211, and 2441 are typical pairs of bulk bcc crystals. On the other hand, the pair 1551, corresponding to a pentagonal bipyramid, is characteristic of icosahedral ordrer. For instance, local order built on a 13-atom icosahedron leads to the occurrence of 1551, 1321, and 2331 pairs.

The microscopic analysis emerging from the data of Table III confirms the composition dependence of the local environment of Mn atoms. At $x=0.14$, the local environment of Mn atoms is dominated by icosahedral and distorted icosahedral inherent structures since the 1551 and 1541 bonded pairs are preponderant. Their sum amounts to 57% of the total number of all bond types, whereas only 32% of 1441, 1431, 1421, and 1422 pairs, related to the tetrahedral local order, are found. At $x=0.2$, the fivefold symmetry decreases but is still quite pronounced since the sum of the 1551 and 1541 bond types is around 50%. The decrease of the fivefold symmetry is mainly due to the decrease of the 1551 bonded pairs. This decrease is still more pronounced at $x=0.4$ since the ratio 1541:1551 at this composition is four times as high as that at $x=0.14$. This result indicates that the SRO at $x=0.4$ is much more complex that the one found in the 13-atom icosahedron. The increase of the ratio 1661:1551 is another signature of the complexity of SRO at $x=0.4$. As already discussed above, the icosahedron is formed by a central atom which has 12 nearest neighbors, all these being joined to it by 12 1551 bonded pairs. Similarly, if the central atom has 14 (or more) neighboring atoms, i.e., $Z14$ (or $Z15$, $Z16$), 12 are joined to the central one by 12 1551 bonded pairs and two (or three or four) by two (or three or four) 1661 bonded pairs. Therefore increasing the ratio 1661:1551 is also a strong indication of an increasing complexity of the Frank-Kasper based polytetrahedral symmetry. Thus all these variations support the occurrence of an increasing complexity of the Frank-Kasper-based polytetrahedral symmetry at $x=0.4$.

We come now to the calculation of the magnetic properties and their evolution as a function of composition. Let us mention that we have treated the spin variable explicitly since we have shown that local moments on Mn atoms have a significant influence on the Mn-Mn distribution in liquid $Al_{80}Mn_{20}$ alloy.[9] Spin-polarized calculations were performed assuming only collinear arrangement of spins for $Al_{1-x}Mn_x$ liquids of different compositions. As already found for $x=0.2$, we did not obtain that the noncollinear state is more stable compared to the collinear one for other compositions.[11] We have argued that the effects due to the exact noncollinear magnetic state of the liquid alloy are not crucial to determine the local geometry around Mn atoms nor its interplay with the appearance of spin polarization. In Fig. 5 are reported distributions of the absolute values of the Mn moments for the three compositions. In our calculations, for $x=0.14$, the distribution is characterized by a narrow peak centered on $2.8\mu_B$ with small moments fluctuating. The distribution becomes wider when the Mn composition increases, characterized by a more asymmetric shape due to an increase of smaller moment values. The calculated average moments are $2.77\mu_B$, $2.55\mu_B$, and $2.63\mu_B$ for $x=0.14$, 0.2, and 0.4, respectively. Let us mention that our calculated values at $x=0.14$ agree well with the experimental values obtained at low Mn compositions,[2] since the latter vary from $2.74\mu_B$ at $T=1180$ K to $2.94\mu_B$ at $T=1280$ K. However, our results do not support the experimental view that only a small fraction of Mn sites carry a moment due to a strong local environment effect, with others being nonmagnetic. Within this experimental scenario, it is believed that the distribution of magnetic and nonmagnetic sites is a consequence of some remanent short-range order in the liquid phases reminiscent of the atomic environment in the crystalline or quasicrystalline phases. From Fig. 5, we can see that this scenario does not hold for the studied compositions even for $x=0.40$ for which the distribution of Mn moments is found to be the largest.

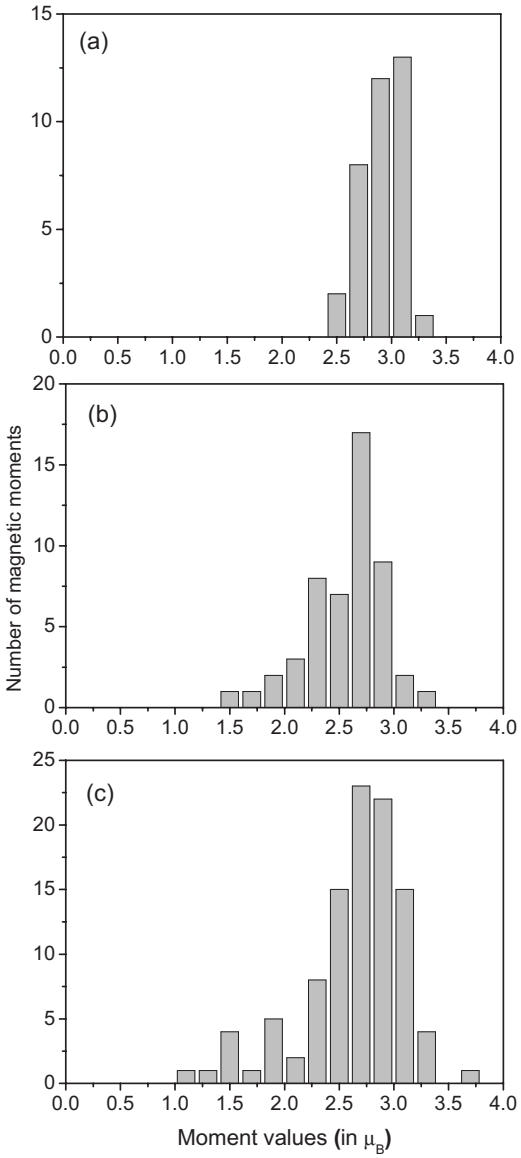

FIG. 5. Distribution of the local magnetic moments of the Mn atoms in $Al_{1-x}Mn_x$ liquids. x= (a) 0.14; (b) 0.2; (c) 0.4.

In fact, the distribution of Mn moments can be explained in terms of thermal fluctuations and chemical variations in the local environment.

The first point to be mentioned is that the formation of localized magnetic moments is not incompatible with the

fivefold symmetry in the liquid state. In fact, the average moment per Mn atom is found to be the highest for $x=0.14$, the liquid phase that displays the most pronounced fivefold symmetry as discussed previously. For this composition, CSRO is also important and both considerations lead to a local icosahedral-type arrangement around Mn atoms. A perfect icosahedral arrangement leads to a central Mn atom surrounded by 12 aluminum atoms and to Al-Mn pairs which are smaller than Al-Al bonds by about 5%, Mn-Mn bonds being larger than Al-Al ones. This local description supports results of Table II for $x=0.14$ and holds more or less for $x=0.20$. In this case, Mn moments are close to those obtained from the single-impurity model,[11] and thermal fluctuations are the relevant parameter which governs the small distribution of localized magnetic moments at $x=0.14$ and 0.20.

The second point is that the situation is quite different at $x=0.4$ and the broadening of the distribution obtained at this composition can be related to the strong increase of Mn-Mn contacts: indeed at this composition, the local topology is characterized by Mn-Mn distances that become similar to Al-Al ones and a very pronounced decrease of the 1551 bond types. Such an evolution may be explained by a strong competition between chemical and magnetic effects. At this composition, Mn-Mn contacts become very important and the presence of Mn-Mn correlations modifies the dilute alloy picture that prevails at $x=0.14$. However, our computational cell size is too small to allow a correct analysis of the spatial correlation between the orientation of Mn moments. Let us mention that the increase of the atomic density at $x=0.4$ may also favor the occurrence of smaller magnetic moments since the Mn atoms become closer to the magnetic-nonmagnetic transition. Indeed, when the atomic density increases, the overlap between orbitals of neighboring atoms increases and the kinetic energy of d states increases too, leading to more and more "delocalized" d states on Mn atoms.[23,24] Such an argument has been used to explain the continuous increase of magnetism with increasing temperature in the liquid $Al_{80}Mn_{20}$ alloy.[11]

IV. CONCLUSION

We have presented a first-principles-based study of $Al_{1-x}Mn_x$ liquids in order to analyze their local order as a function of composition. The determination of the Bhatia-Thornton partial structure factor $S_{cc}(q)$ gives evidence of a pronounced chemical SRO for all studied compositions. For $x=0.14$ and 0.2, compositions from which quasicrystalline phases may be formed by quenching techniques, our results, based on the determination of partial coordination numbers and the common-neighbor analysis, clearly show the predominance of the icosahedral local symmetry around Mn atoms. For $x=0.4$, a composition outside the quasicrystal-forming composition range, we find that the local arrangement between Mn-Mn pairs changes significantly as compared to what occurs at $x=0.2$. We also observe that the fivefold local symmetry is still present but leads to a short-range order which is much more complex than the one found at $x=0.2$ or 0.14. Then we conclude that a strong icosahedral ordering in the liquid phase is a preponderant feature of the quasicrystalline phase formation for Al-Mn alloys using fast quenching techniques.

Concerning the dynamics, we have analyzed the mean-square displacement as a function of time for each species and calculated the partial self-diffusion coefficients from the corresponding velocity autocorrelation functions. We have found that the cage effect becomes more pronounced, and the self-diffusion coefficients of both species take similar values, as the concentration of Mn atoms increases.

For $x=0.14$ and 0.20, Mn atoms carry large magnetic moments, characteristic of the single-impurity limit and in agreement with experimental values. At $x=0.40$, the wide smearing of the calculated distributions of the magnitude of Mn moments can be related to the effect of atomic density increase and a strong competition between chemical and magnetic effects, leading to a local structure more complex than that of the icosahedron.

ACKNOWLEDGMENTS

We acknowledge PHYNUM-CIMENT-UJF as well as IDRIS-CNRS (Project No. 061706) for computational resources.

[1] M. Maret, A. Pasturel, C. Senillou, J. M. Dubois, and P. Chieux, J. Phys. (France) **50**, 295 (1989); M. Maret, P. Chieux, J. M. Dubois, and A. Pasturel, J. Phys.: Condens. Matter **3**, 2801 (1991); M. Maret, T. Pomme, A. Pasturel, and P. Chieux, Phys. Rev. B **42**, 1598 (1990).

[2] F. Hippert, M. Audier, H. Klein, R. Bellissent, and D. Boursier, Phys. Rev. Lett. **76**, 54 (1996); V. Simonet, F. Hippert, H. Klein, M. Audier, R. Bellissent, H. Fischer, A. P. Murani, and D. Boursier, Phys. Rev. B **58**, 6273 (1998); V. Simonet, F. Hippert, M. Audier, and R. Bellissent, *ibid.* **65**, 024203 (2001).

[3] R. Phillips, J. Zou, A. E. Carlsson, and M. Widom, Phys. Rev. B **49**, 9322 (1994).

[4] J. Hafner and M. Krajci, Phys. Rev. B **57**, 2849 (1998).

[5] L. Do Phuong, D. Nguyen Manh, and A. Pasturel, Phys. Rev. Lett. **71**, 372 (1993).

[6] A. M. Bratkovsky, A. V. Smirnov, D. Nguyen Manh, and A. Pasturel, Phys. Rev. B **52**, 3056 (1995).

[7] A. V. Smirnov and A. M. Bratkovsky, Phys. Rev. B **53**, 8515 (1996).

[8] M. Maret, L. Lancon, and L. Billard, J. Phys. I **3**, 1873 (1993); J. Phys.: Condens. Matter **6**, 5791 (1994).

[9] N. Jakse, O. Lebacq, and A. Pasturel, Phys. Rev. Lett. **93**, 207801 (2004); J. Chem. Phys. **123**, 104508 (2005).

[10] J. D. Honeycutt and H. C. Andersen, J. Phys. Chem. **91**, 4950 (1987).

[11] N. Jakse, O. Lebacq, and A. Pasturel, Europhys. Lett. **74**, 275 (2006).

[12] Y. Wang and J. P. Perdew, Phys. Rev. B **44**, 13298 (1991).

[13] G. Kresse and J. Furthmüller, Comput. Mater. Sci. **6**, 15 (1996); Phys. Rev. B **54**, 11169 (1996).
[14] G. Kresse and D. Joubert, Phys. Rev. B **59**, 1758 (1999).
[15] S. H. Vosko, L. Wilk, and M. Nusair, Can. J. Phys. **58**, 1200 (1980).
[16] The values obtained here for *D* correct the first estimate based on short runs reported in N. Jakse and A. Pasturel, Mod. Phys. Lett. B **20**, 655 (2006).
[17] D. Alfe, G. Kresse, and M. J. Gillan, Phys. Rev. B **61**, 132 (2000).
[18] F. H. Stillinger and T. A. Weber, Phys. Rev. A **25**, 978 (1982).
[19] M. Asta, V. Ozolins, J. J. Hoyt, and M. van Schilfgaarde, Phys. Rev. B **64**, 020201 (2001).
[20] A. Baranyai and D. J. Evans, Phys. Rev. A **40**, 3817 (1989).
[21] S. Sachdev and D. R. Nelson, Phys. Rev. Lett. **53**, 1947 (1984); Phys. Rev. B **32**, 4592 (1985).
[22] C. N. J. Wagner and H. Ruppersberg, At. Energy Rev. **1**, 101 (1981).
[23] G. Trambly de Laissardiere and D. Mayou, Phys. Rev. Lett. **85**, 3273 (2000).
[24] G. Trambly de Laissardiere, D. Nguyen Manh, and D. Mayou, Prog. Mater. Sci. **50**, 679 (2005).